Tectonophysics 773 (2019) 228233

Contents lists available at ScienceDirect

Tectonophysics

journal homepage: www.elsevier.com/locate/tecto

Time-dependent modelling of a mountain front retreat due to a fold-to-fault controlled lateral spreading

P. Alfaro[a], J. Delgado[b], C. Esposito[c], F. García Tortosa[d], G.M. Marmoni[c,*], S. Martino[c]

[a] Department of Earth Sciences and Environment, University of Alicante, P.O. Box 99, 03080 Alicante, Spain
[b] Department of Construction Engineering, University of Alicante, P.O. Box 99, 03080 Alicante, Spain
[c] Earth Sciences Department of "Sapienza" University of Rome and CERI - Research Centre for Geological Risks, P.le Aldo Moro n.5, I-00185 Rome, Italy
[d] Department of Geology, University of Jaén, Campus Las Lagunillas, 23071 Jaén, Spain

ARTICLE INFO

Keywords:
Lateral spreading
Betic cordillera
Rock mass
Slope stability
Multi-modelling
Numerical modelling

ABSTRACT

The Eastern Betic Cordillera (Spain) exemplifies at the Sierra de Aitana an impressive case of lateral spreading which involves a mountain anticline ridge dislodged by a post-orogenic extensional tectonic. The deep trenches testify the ongoing gravitational slope deformation featured by a rock mass lateral spreading. The Sierra de Aitana anticline ridge was dislodged along a normal fault zone which generated a scarp with a kilometric lateral continuity. The lateral spreading originated because Eocene limestone overlays Eocene marls, inducing a continuous evolution over time due to visco-plastic deformations and isolating huge prismatic blocks. To quantify the creep-driven stress-strain effects at Sierra de Aitana ridge, the mechanical and rheological parameter values of the involved rocks were quantified through field and laboratory tests which allowed to constrain an engineering-geological model based on equivalent-continuum approach. A stress-strain numerical modelling aimed at back-analysing the sequential morpho-structural evolution of the Sierra de Aitana anticline-ridge was performed by reproducing the retreat of the ridge front and the time succession of faults (re)activations. A time-dependent solution was approached by assuming a time-dependent creep configuration of the modelling and a parametric solution adopted to calibrate rock mass rheology, also taking into account: tectonic displacement due to the Aitana normal fault system by simulating these element as interface in the discretized domain; influence of pre-existing joint sets by assuming a main anisotropy in the elasto-plastic failure solution; admissible variations of the regional stress-field related to compressive and extensional phases and a generalised visco-plastic behaviour representing the ductile marls. The numerical modelling outputs that the lateral spreading mainly evolved as a creep-driven process while stress-release induced by tectonic activity is not sufficient to justify the observed landforms. The obtained results highlight a not negligible role of inherited structural elements for regulating the time evolution of the ongoing gravitational process at the Sierra the Aitana anticline.

1. Introduction

The onset and evolution up to failure of slope-scale gravity-driven deformations are strongly controlled by geological and morphological features, such as the presence of lithologies with stiffness contrasts and steep slopes which predispose to slope deformations. The latter can be produced by either erosion or tectonics (or their combination in space and time), resulting in over-steepened slopes that are kinematically unconstrained at toe and free-to-move in lateral directions. Where structural frameworks allow the co-existence of kinematics and geological predisposing factors lateral spreading can onset and develop, driven by the time-dependent deformation of weak and ductile layers.

Lateral stress unloading, resulting by generations of free-face escarpments, can be recognised as main mechanism driving gravitational instabilities (Ballantyne, 2002; Bozzano et al., 2008). In the case of rock-slope lateral spreading (Pasuto and Soldati, 1996; Hungr et al., 2014) essential requisite is the presence of deformability contrast between a stiff rock mass and a softer and ductile underlying material (Hutchinson, 1988; Rohn et al., 2004), the presence of a free-face which accommodates the horizontal movement and joint opening in the rock slab (Canuti et al., 1990; Bozzano et al., 2010; Borgatti et al., 2015; Spreafico et al., 2017). The slow spreading exerts as a single near-horizontal movement of coherent blocks or by multiple retrogressive sliding accomodated through visco-plastic deformations (Bozzano et al., 2013; Bois et al., 2015).

Based on these geological pre-requisites, regional meso-scale folds

* Corresponding author.
E-mail address: gianmarco.marmoni@uniroma1.it (G.M. Marmoni).

https://doi.org/10.1016/j.tecto.2019.228233
Received 5 August 2019; Received in revised form 30 September 2019; Accepted 20 October 2019
Available online 23 October 2019

(Scarascia Mugnozza et al., 2006) and ridge-bounding extensional fault systems (Kellogg, 2001; Esposito et al., 2013; Bianchi Fasani et al., 2014) can represent the most predisposing structural arrangement where these deformations take place. Fault-to-fold combinations, i.e. the existence of faulted fold limbs, can even more represents the morpho-structural setting where rock spreading can evolve (Di Luzio et al., 2004a, 2004b; Della Seta et al., 2017).

In such cases, folds and faults provide respectively the inherited passive structural framework (e.g. coupling of geological media, dip-slope bedding attitude, jointing conditions) and an active role of trigger, causing a stress-release which controls timing of slope deformations (Ambrosi and Crosta, 2006; Esposito et al., 2014). For these reasons, the onset and development of gravity-induced slope deformation, as well as the mechanism and kinematics driving their evolution, are regulated by the proceeding of morphological and morpho-structural steps of evolution of mountain slopes, related to both tectonic and erosional processes (Agliardi et al., 2009; Bianchi Fasani et al., 2011).

Due to the large spatial and temporal scales of processes regulating slope-scale morphogenesis, in addition to geo-structural framework, the time-dependent rheology of the involved materials cannot be neglected (Della Seta et al., 2017). In order to infer rheological parameters and back-analyse the stress-strain interactions in slope deformations, a correct definition of the geomechanical properties of the rock mass, as well as a calibration of a morpho-structural evolutionary model of slope system is required and a detailed transposition via multi-stage time-dependent numerical models is advised for constraining slope deformative style (Martino et al., 2017).

For these reasons the integration of multidisciplinary methods based on geomorphological (Bozzano et al., 2016), morpho-structural, geomechanical (Discenza et al., 2011; Marmoni et al., 2017) and numerical (Bozzano et al., 2012; Della Seta et al., 2017) contributions in a multi-modelling scheme (Martino et al., 2017) is necessary.

This study tests a multi-modelling approach combining morpho-structural and geomechanical elements in a stress-strain multistage numerical analysis of the Sierra de Aitana lateral spreading; a block-disjointed 2D numerical domain was resolved availing of mesh-interfaces, reproducing timing and displacements of the major tectonic phases which dictated the onset of the gravitational process.

2. The Sierra de Aitana case study

2.1. Morphostructural framework

The Eastern Betic Cordillera (Spain) shows at the Sierra de Aitana (Alicante province) an impressive case of lateral spreading which involves an anticline mountain ridge, composed of Eocene and Upper Cretaceous carbonates and calcareous marls.

The structure of the Sierra de Aitana is an E–W open symmetric anticline with a wavelength of 5 km and around 20° dipping limbs, belonging to a regional succession of E–W to ENE–WSW folds and thrusts with wavelengths varying between 3 and 6 km (De Ruig, 1992). The Sierra de Aitana ridge is constituted by a deformed sedimentary cover of marine calcareous Mesozoic and Cenozoic rocks belonging to the Prebetic Domain of the Betic Cordillera External Zone (Fig. 1; Sanz de Galdeano and Alfaro, 2004). This sedimentary cover detached from a Paleozoic basement along Triassic evaporites and clays during the early–middle Miocene (De Ruig, 1992).

The stratigraphic succession includes from the base to the top: i) 300-m thick Upper Cretaceous biomicrites, bioclastic calcarenites, cropping out in the anticline core; ii) Upper Cretaceous marls and limestones; iii) Eocene green marls and clays, with thickness varying between 50 and 200 m; iv) Middle Eocene limestones constituted by biomicrites, biosparites and calcarenites with a thickness varying between 40 and 300 m. This sequence, characterised by a thick Eocene limestone overlying marls of the same age, constitutes the rheological coupling that drove the lateral spreading process. Quaternary unconsolidated material such as rock debris deposited in talus slopes and debris cones originated by weathering and landslides (e.g. mainly rock fall, rockslides and topples), partially cover the slopes of Sierra de Aitana ridge.

The Sierra de Aitana anticline was cut and dislodged by several normal faults, probably originated during a late Miocene extensional tectonic phase related to the opening of the Valencia trough (Marco Molina, 1990; De Ruig, 1992; Yébenes et al., 2002). Among these, the Sierra de Aitana master fault generated in the southern limb of the fold a 150 m high scarp which is approximately parallel to the fold hinge line with a kilometric lateral continuity. At the surface, the main fault plane outcrops along the northern slope of the Sierra de Aitana with an average dips of 45 °N and an estimated net slip up to 400 m (Delgado et al., 2011). These normal faults reflect in a stair-shaped morphology, where the Sierra de Aitana main fault produces the main steep mountain front. Several high angle joint sets affect the Sierra de Aitana fold with a spacing from 1 up to 10 m and an oblique and symmetrical distribution with respect to the fold hinge, suggesting a genetic relationship associated with folding (Delgado et al., 2011). Close to the present mountain scarp, the most recent gravitational processes reactivate these conjugate joints producing large opening fissures, fractures and veins with a segmented morphology. The average strike of these conjugate fractures is almost parallel to the slope face. Large veins are filled with speleothems, which indicate an extremely slow opening.

2.2. Geomorphological evidences related to the lateral spreading

Due to the geological setting where Eocene limestone (EL) overlays Eocene marls and clays (EM) a lateral spreading originated, isolating huge prismatic blocks (Fig. 2a) shaped by the aforementioned discontinuity sets (Fig. 2b). This continuous evolution has turned in the generation of a nearly vertical EL scarp extended down to the underlying EM and deep trenches (Fig. 2c), which are extensively hidden by debris talus deposits. The EL slab is dislodged in several blocks of variable size from hundreds to tens of thousands of cubic meters (Fig. 2d) that have detached and laterally moved away from the scarp, generating secondary scarps and graben-like depressions. Related block slides (*sensu* Varnes, 1978) have also sunk and back tilted with respect to the stable limestone slab, showing a slight tilting angle of about 5° with a vertical component of movement which reached up to 20 m, accommodated by the deformable EM (Fig. 2a). Features related to sliding and shearing as slicken lines were recognised on fracture walls by Delgado et al. (2011).

NE of the spreading zone, in the most spectacular sector (locally known as “Simas de Partagat”), several rock blocks are isolated from the top plateau by 40 m deep and 20 m wide trenches which demonstrate the main horizontal component of the displacement. The opening of trenches resulted by the spreading of the stiff rock plateau which accommodated the horizontal displacements involving the softer marls. The opening of trenches testifies the creep-driven evolution of the gravitational slope deformation (Fig. 2c, d).

As an ultimate process, the dislodged rock blocks gradually collapsed moving several tens of meters far from the top of the cliff slope. According to Delgado et al. (2011), the distribution of rock blocks along the slope testifies a continuous and concatenated failure mechanism. The collapsed rock blocks produce a large debris cover which actually hides the contact between the limestones and the marls, responsible for a total amount of front retreat of around 400 m from the Sierra de Aitana fault trace to the actual mountain front (Delgado et al., 2011).

As reported by Delgado et al. (2011), the satellite DInSAR monitoring carried out over a time span of 11 yr from January 1997 to October 2008, revealed to date very low deformation rates and negligible cumulative displacements related to the deformations.

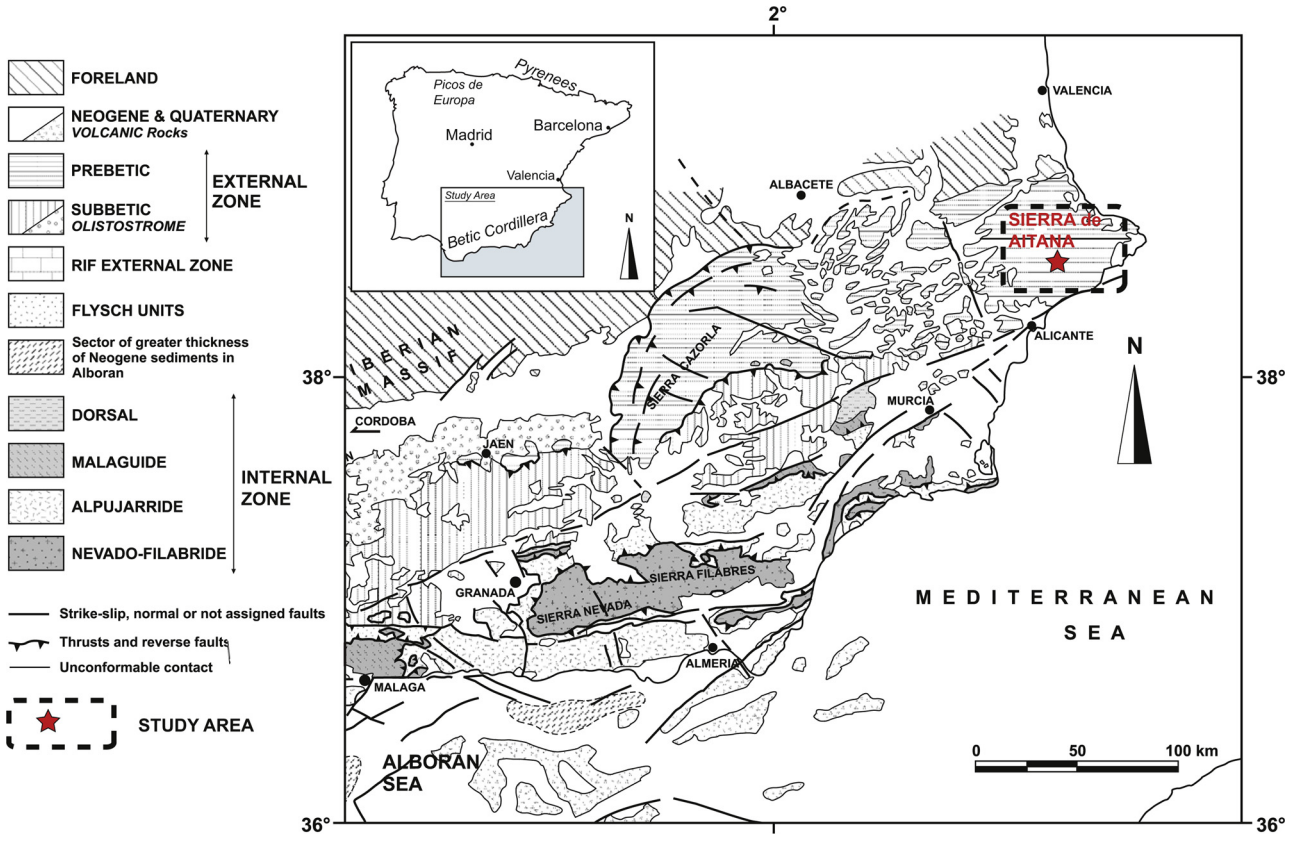

Fig. 1. Geologic sketch of Sierra de Aitana in the Betic Cordillera, modified after Sanz de Galdeano and Alfaro (2004).

3. Materials and methods

The back-analysis of gravity-driven processes acting on large spatial and temporal scales require a valid definition of i) "internal" factors, such as the rheological parameters of the involved materials and ii) "boundary" conditions controlling the onset of slope-scale deformations. Among the main boundary controlling factors, a key role is played by the morpho-structural evolution of slope systems, resulting by either erosion or tectonics, which is able to modulate the stress field acting on the slope and, thus, the deformative response. For these reasons a multi-modelling approach (*sensu* Martino et al., 2017) was adopted to model the Sierra de Aitana lateral spreading initiation and evolution, defining timing and displacement of major tectonic phases, delineating an engineering-geological model and characterising the geomechanical properties of the involved materials to be transposed in multi-stage numerical models. In the following section, the main aspects and solutions adopted throughout these fundamental steps will be described and analysed.

3.1. Morpho-structural evolutionary model

To constrain timing and displacements of major tectonic phases, a morpho-structural evolutionary model of the Sierra de Aitana anticline was resolved (Fig. 3), supporting a geological cross-section proposed by Delgado et al. (2011) (Fig. 3a). The main tectonic phases are in agreement with those proposed by De Ruig (1992) and are supported by integrated geomorphological stratigraphical, sedimentological and geophysical observations reported by Yébenes et al. (2002) in the continental shelf and neighbouring offshore of Betic Cordillera External Zone.

The proposed landscape evolution model indicate that these normal faults were active mainly during the late Miocene (Yébenes et al., 2002). Basing on the available data, a 2D sequential morpho-evolutionary model of the Sierra de Aitana ridge sector was proposed, trying to assess their role in the time-evolution of mountain front retreat and define a time-window where the lateral spreading of Sierra de Aitana could have evolved.

The morpho-structural evolution of the ridge starts with folding of the limestone and marly sedimentary cover, which in this area is reported to the Lower to middle Miocene period (De Ruig, 1992). During Late Miocene (Fig. 3b) the extensional tectonic phase dissected the sedimentary succession generating the present state main scarp of the ridge. The main dislodgement of the Sierra de Aitana fault overcomes 300 m, although rates of activity are unknown to date.

Faulting along secondary planes F2 and F3 took place since the end of main Aitana fault activity (Fig. 3c), which, according to the calibrated structural cross-section, cumulated a tectonic displacement of about 80 m and 40 m for F2 and F3, respectively (Fig. 3d). Because of lacks of detailed information about timing of activity of secondary faults, a precise definition of age of fault displacements is arduous. Despite this irresolution, the net effect of stress-release induced by fault dislodgement on the rock cliff was rigorously evaluated.

To overcome this time uncertainty, a double hypothesis in timing of fault activation was proposed, considering a synchronous activation of the two faults with respect to the modelled timescales. Two opposite end-member solutions of F2 and F3 activation, namely "A" and "B" were considered, trying to evaluate their effect in dictating occurrence of rock failures. The two different timing hypotheses are detailed in Section 3.3. In this time-range the slope-scale Aitana lateral spreading took place. During the Plio-Quaternary age, minor small-scale gravitational processes contributed to the landscape carving of the relief, giving rise to present state of the slope.

3.2. Engineering-geological model

To back-analyse the gravity-driven evolution of the Sierra de Aitana

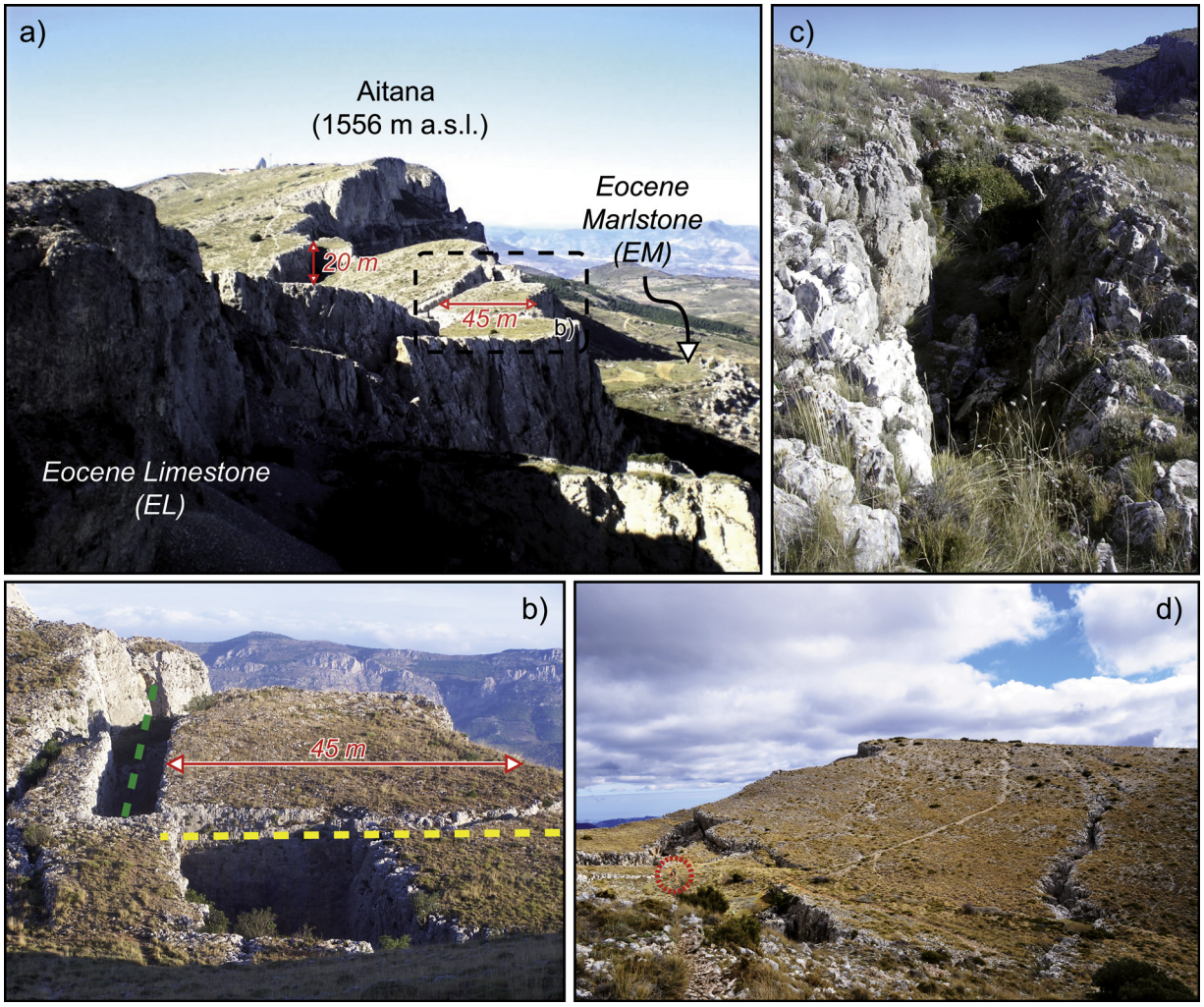

Fig. 2. a) E–W view of the overall lateral spreading process involving Eocene Limestone (EL) and Marls (EM) along several kilometres of the Sierra Aitana ridge; b) rock block detachment of decametric-scale prismatic blocks exploiting two major pervasive joint sets with dip direction/dip orientation of 355/79 (green dashed line) and 85/88 (yellow dashed line); c) detailed view of one of the widening trenches; d) view from the top of a dislodged rock block rounded by trenches with metrics dimensions in wide and length. The reader is referred to people in red circles as reference scale.

ridge, an engineering-geological model of the anticline structure was defined based on laboratory tests and geomechanical field surveys. Limestone and marls were sampled NW of the Simas de Partagat, just at the foot of the limestone slab, where they are not covered by debris deposits. Lithologies have been characterised through a suite of laboratory investigations (summarised in Table 1). Physical and mechanical properties of both EM and EL were derived for the intact rock and then scaled to the rock masses by equivalent continuum approach (Sridevi and Sitharam, 2000; Sitharam et al., 2001). For this purpose, the most relevant parameters describing jointing conditions, like orientation, spacing, JRC, JCS and volumetric joint density (Jv) of EL were based on field measurements (Marmoni, 2011) according to ISRM (1978) standards and basing on stereoplot dataset reported by Delgado et al. (2011).

The laboratory activity included uniaxial compressive strength tests (UCS), indirect tensile tests ("Brazilian" test), direct shear tests, ultrasonic velocity tests and unit weight measurements (Table 1). On the EM, particle size analysis and direct shear tests were also performed according to ASTM standards.

By combining data from laboratory tests for the intact rock with geomechanical scanlines from the outcropping rock mass (expressed by Jv), mechanical parameters of the rock masses were derived directly using geomechanical parameters obtained from exposed rock surveys and adopting an equivalent continuum approach where a Joint Factor (J_f) (Ramamurthy, 1994; Sridevi and Sitharam, 2000) is defined through the equation:

$$E_{j0} = \exp(-1.15*10 - 2J_f)E_{i0} \quad (1)$$

where Ei_0 represent the Young modulus at null confinement. Elastic moduli of fractured rock masses were derived at non-zero confining pressure (E_j) by the equation:

$$E_j = E_{j_0}/1 - \exp[-0.1\sigma_{c\,j}/\sigma_c] \quad (2)$$

where σ_c represents the confining pressure and σ_{cj} express the UCS of the jointed rock, calculated by negative exponential function by the UCS of intact rock (σ_{ci}) as reported in the equation:

$$\sigma_{c\,j} = \sigma_{ci}[0.04 + 0.89\exp(-J_f/161)] \quad (3)$$

The mechanical parameters values were derived from the rock matrix according to Hoek-Brown criterion (Hoek et al., 2002), considering geotechnical properties function of the stress-field existing within the slopes. At this aim, two sets of parameter values were assumed, considering admissible variations of the regional stress-field over a range of values representative of compressive and extensional phases. Such a stress-field change is based on variations of the horizontal to vertical stress ratio (K) ranging between 0.6 and 0.4, as already proposed in literature (Della Seta et al., 2017).

Deformative behaviour of the thick EL slab was finally distinguished

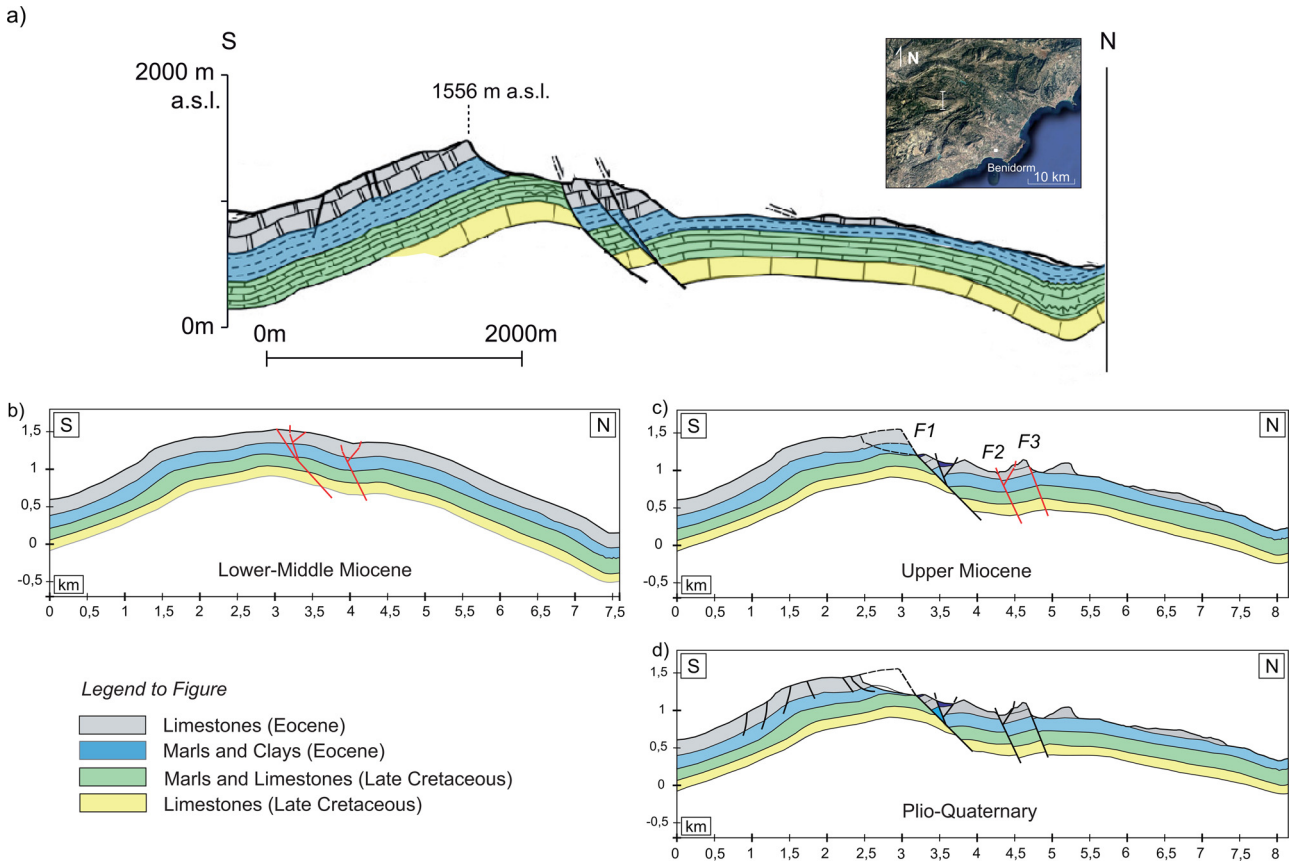

Fig. 3. a) Geological cross-section (modified after Delgado et al., 2011) and reconstructed morpho-evolutionary model of the Sierra de Aitana anticline since Lower-Middle Miocene (b) to Plio-Quaternary (d). The activity timing of tectonic elements is reported by red colouring of faults planes. (For interpretation of the references to colour in this figure, the reader is referred to the web version of this article.)

Table 1
Type and number of laboratory tests performed.

Test Type	*Number of tested specimens from EL*	*Number of tested specimens from EM*
Particle Size	–	1
Unit Weight	3	3
Ultrasonic Velocity	20	10
Direct Shear Test	–	2
Uniaxial Compressive Strength	10	6
Indirect Tensile Strength	4	4

defining three lithotechnical zones related to depth, i.e. at among 0–50, 50–100 and 100–200 m below the ground level (Table 2) and characterised by increasing values of elastic moduli with confining pressures.

According to Esposito et al. (2007) and Della Seta et al. (2017), major anisotropies in limestones predisposing the rock mass to failure were also considered, attributing strength properties based on the Barton and Choubey (1977) criterion, while joint cohesion was fixed to a value of one order of magnitude lower than the intact rock. The adopted values for mechanical parameters are summarised in Table 2.

3.3. Stress-strain numerical model

To reconstruct the slope evolution of the Sierra de Aitana ridge in terms of stress–strain analysis, a numerical modelling was carried out through the finite difference code FLAC 2D 7.0 (Itasca, 2011), performing a sequential analysis which reproduced the main steps of the morpho-structural evolution along the geological cross-section of Fig. 3, representative of geo- and morpho-structural conditions that could be assumed before the Sierra de Aitana fault activation (Fig. 3a). A 870 × 380 square grid with a resolution of 10 m was adopted to discretise the numerical domain, while lateral boundaries were artificially extended up to about 500 m to avoid boundary effects or computational errors (Fig. 4). Mesh resolution was settled-up basing on dimension of finest geometrical elements to be modelled, defining it as the best compromise between model resolution and calculation time. No systematic sensitivity analysis to mesh resolution was performed. As an infinite half-space was assumed, roller boundary conditions along the lateral boundaries of the numerical domain were fixed, i.e. the horizontal displacements were avoided, while both vertical and horizontal displacements were avoided at the model bottom during the mechanical equilibrium. After consolidations, bottom of the model in hanging-wall regions were leaved free to move in vertical direction, allowing rigid translation of the mesh along fault plane.

Faults planes were primary reproduced availing of a single- or bi-planar interface geometry models, analysing the strain-field at elasto-plastic equilibrium, by leaving free (i.e. unglued) interface during calculation. Based on the derived results for a biplanar fault-path model, where a marked counter-clockwise rotation of shallow mesh-regions and a consequent overlap of mesh-elements along interface were experienced, a single-planar interface model was adopted to reproduce the lateral spreading process. This solution, therefore, revealed the only one suitable for reproducing fault displacement at these scales and for slope-instability analyses purposes.

To calibrate the visco-plastic rheology of the rock mass, the mountain front retreat caused by the lateral spreading was regarded as a possible target. Therefore, the stress-strain sequential numerical modelling was performed by adopting a time-dependent creep configuration and following a parametric analysis. At this aim, the following

Table 2
Derived mechanical parameters and constitutive laws adopted for both rock mass and joints for the adopted engineering geological zonation. Models (constitutive models): el = elastic; mc = Mohr-Coulomb; ub = ubiquitous joint; cvisc = Burger creep. φ = friction angle. c = cohesion. t = tensile strength. K = bulk modulus. G = shear modulus. Jang = joint dip angle. Jfr = joint friction angle. Jcoh = joint cohesion. Jten = joint tensile strength.

Compressive Initial Stage

Unit	Depth Zone (m)	Models	Rock Mass						Ubiquitous Joint			
			Density (kg/m^3)	K (Pa)	G (Pa)	c (Pa)	t (Pa)	φ (°)	Jang (°)	Jcoh (°)	Jten (°)	Jfr (°)
EL	0-50	ub	2614	8.72E+09	4.17E+10	2.41E+06	1.80E+06	53	79	4.44E+05	3.39E+05	52.6
EL	50-100	ub	2614	8.79E+09	4.20E+10	2.52E+06	2.02E+06	51	79	4.53E+05	4.10E+05	47.8
EL	100-200	ub	2614	9.52E+09	4.55E+10	2.89E+06	2.67E+06	47	79	4.74E+05	4.77E+05	44.8
EM	–	mc, cvisc	2470	1.63E+10	3.48E+09	1.77E+05	1.11E+06	27	–	–	–	–
CM	–	mc	2480	1.53E+08	9.15E+07	9.22E+06	1.48E+07	32	–	–	–	–
CL	–	el	2700	9.52E+11	4.55E+12	–	–	–	–	–	–	–

Extensional Stage

Unit	Depth Zone (m)	Models	Rock Mass						Ubiquitous Joint			
			Density (kg/m^3)	K (Pa)	G (Pa)	c (Pa)	t (Pa)	φ (°)	Jang (°)	Jcoh (°)	Jten (°)	Jfr (°)
EL	0-50	ub	2614	6.98E+09	3.34E+10	1.20E+06	8.10E+05	56	79	4.44E+05	3.39E+05	52.6
EL	50-100	ub	2614	6.99E+09	3.34E+10	1.33E+06	1.03E+06	52	79	4.53E+05	4.10E+05	47.8
EL	100-200	ub	2614	7.20E+09	3.44E+10	1.62E+06	1.46E+06	48	79	4.74E+05	4.77E+05	44.8
EM	–	mc, cvisc	2470	1.50E+10	3.22E+09	1.76E+05	1.11E+06	27	–	–	–	–
CM	–	mc	2480	1.53E+08	9.15E+07	9.22E+06	1.48E+07	32	–	–	–	–
CL	–	el	2700	9.52E+11	4.55E+12	–	–	–	–	–	–	–

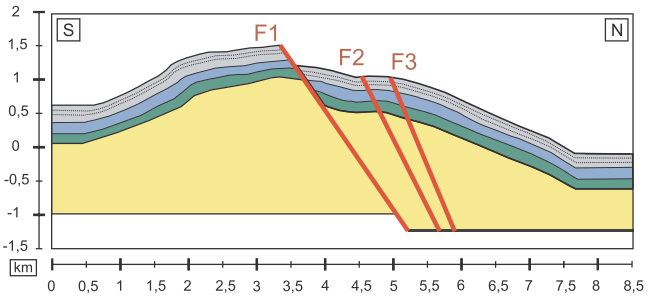

Fig. 4. Sketch of numerical model reproduced by rigid mesh translation at stage c) of the morpho-evolutionary sequence reported in Fig. 3.

conditions were assumed:

i) the Sierra de Aitana normal fault displacements were obtained through a time- and space-controlled rigid translation of hanging-wall regions of the model (Fig. 5);
ii) the timing of the gravity-induced slope deformations was influenced by the progressive fault displacements (along interfaces F2 and F3);
iii) the influence of pre-existing joint sets in rock failure was accounted for by assuming a main anisotropy in the elasto-plastic failure criterion (i.e. using a ubiquitous joint constitutive model);
iv) admissible variations of the regional stress-field were related to compressive and extensional phases;
v) a generalised visco-plastic rheological model was adopted to represent the mechanical behaviour of the ductile EM overlying the rigid elasto-plastic EL and a range of viscosity values varying from 10^{20} up to 10^{22} Pa·s was assumed.

Because of the uncertainty existing in both timing and slip rates of the Sierra de Aitana fault systems, a linear slip rate was roughly assumed which can be regarded as the most precautionary hypotheses. Despite the listric pattern of the main faults of the Sierra de Aitana structural system, (F1) (Delgado et al., 2011), these elements were numerically reproduced assuming a mesh interface with planar path,

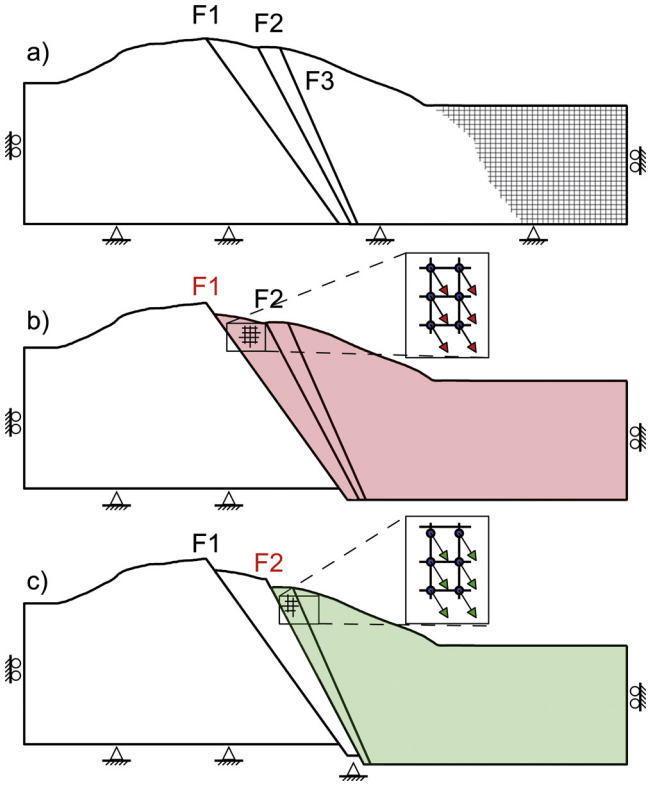

Fig. 5. Sketch of mesh rigid translation adopted in the FLAC 2D v. 7.0 code (Itasca cons.) to simulate tectonic displacement along fault reproduced by mesh interfaces. Tectonic displacements were constrained in time and magnitude according to morpho-structural evolutionary model. Boundary conditions across different stages are reported. Rigid translation were imposed on all the nodes of the grid belonging to the hanging-wall of major faults F1 (a) and F2 (b) reproducing the sequential activation of fault plane since the initial undeformed stage (Fig. 3b), until Upper Miocene (Fig. 3c) and Plio-Quaternary extensional phases (Fig. 3d).

which was extended to the model bottom (Fig. 5a) as the here modelled depth is limited to some hundreds of meters.

The morpho-structural evolution of the Sierra de Aitana anticline slope was simulated by a multi-stage sequential numerical modelling, starting from the last activation of the Aitana fault (Late Miocene). To output the stress-strain effects due to the fault activation, the lowering of the hanging-wall respect to the footwall was obtained as a rigid dip-slip displacement involving a single portion of the mesh (Fig. 5b and c). This solution differs from already experienced literature approach (Bianchi Fasani et al., 2011), where the effect due to the stress release was reproduced by a discrete step-by-step variation of the model geometry. Such a solution allows to discretise the fault activation in several stages and to output variations of the stress field and solve the resulting strain field over time, without nullifying numerical regions of the model which causes an instantaneous release with a consequent rebound of the unconfined portions of the numerical domain.

As detailed information about the age of activity of secondary faults (F2 and F3) lacks, in order to test the active role of fault in driving the evolution of the lateral spreading at Sierra de Aitana, two hypotheses of timing for fault activation were assumed, representing two end-member respect to the admissible range of available timing data.

In the first hypothesis (A), an early activation of faults up to 2 Myr after F1 was assumed, considering a sequential activation of faults in Upper Miocene. In the second hypothesis (B), a late activation of F2 and F3 was reproduced (age 2.5–3 Ma), considering an activation occurred during a Plio-Quaternary extensional phase as inferred by Rey and Fumanal (1996) or Roselló and Fumanal (1999). Following this approach, the sensitivity to gravity-induced processes controlled by fault activation at different stage of slope deformation was tested, trying to weight its role in inducing rock failure occurrence.

A pervasive steeply dipping joint set within the rock mass was considered in all the models according to a ubiquitous joint constitutive model for the EL zones, so providing a major anisotropy to the elasto-plastic mechanical solution. A southward-dipping (i.e counterslope-dipping) joint set was also taken into account to avoid overestimation of the front retreat and to better understand the role of the anticline structure in the mechanism of the lateral spreading.

In the solution for mechanical equilibrium, admissible variations of the regional stress-field related to compressive and extensional phases were taken into account. The stress field which resulted in the numerical domain was constrained to the initial regional compressive stress field applying increased elastic moduli proportional to the confining stress acting at the different depth. The progressive reduction of the confining stress resulting from the Sierra de Aitana fault activation under a extensional stress field was modelled by reducing the elastic moduli (Table 2) in proportion with horizontal to vertical stress (K) ratios (Bianchi Fasani et al., 2011; Della Seta et al., 2017). After an initial stage representative of compressive stress-states existing within slope at end of folding (Fig. 3b), an instantaneous variation of K-ratio was applied after the simulated fault displacement (Fig. 3c). Mechanical equilibrium conditions were thus updated before the time-dependent calculations, in order to guarantee numerical stability.

The numerical solutions under creep configuration were obtained by assuming a time step duration of 630 Ms (almost equal to 20 yrs) and by attributing viscosity values for the visco-elastic Maxwell element of the Burger model varying in the range 10^{20}–10^{22}Pa·s. The time step durations were defined considering the maximum creep daytime applicable at the minimum viscosity to ensure numerical stability and derived by the viscosity/shear modulus (η/G) ratio.

Moreover, the viscosity value attributed to the visco-plastic Kelvin-Voigt element of the Burger model was increased of one order of magnitude, with respect to that of the Maxwell element, as it considered as representative for the visco-elastic rheological behaviour of the intact rock (Bozzano et al., 2012).

Basing on these assumptions, a back-analysis was performed adopting a visco-plastic rheological behaviour represented by the Burger model with the aim of calibrating the mechanical parameter values attributed to the EM zones; the viscosity value was best-tuned by comparing the numerical modelling outputs with the evidences from the landforms produced by the morpho-structural evolution of the lateral spreading (i.e. entity of the total front retreat, size of mobilised volumes, correspondence of opened cracks and trenches with tensile stresses).

4. Numerical modelling results

Lateral spreadings are often driven by the overlaying of litho-technical units characterised by different mechanical behaviours; such a juxtaposition causes horizontal displacements of the stiff rock-cap under the effect of gravity (Bozzano et al., 2008 and reference therein).

In the here considered case-study, UCS tests performed on the two involved geological formations (EL and EM) allowed to derive their stiffness contrast (see Table 2) which can be regarded as responsible for the gravity-driven lateral spreading at Sierra de Aitana ridge, together with an admissible visco-plastic behaviour of the EM formation (Fig. 2).

The here performed stress-strain numerical modelling was focused on quantifying the role of both time-dependent rheology of EM and the structural evolution of the slope related to an initial folding and secondary repeated normal fault activations, in the lateral spreading occurrence.

To validate the back-analysis, a geomorphological target was adopted verifying by convergence the entity of the simulated total mountain front retreat (via numerical approach) compared with the actual distance of the wall respect the fault plane (i.e. observed front retreat). The simulated total front retreat was estimated by cumulating the width of the limestone portions which undergone plasticity as it resulted from the lateral spreading.

The yielding zones of the numerical domain were subsequently removed (but only in the case that the involved meshes had a spatial continuity dislodging individual rock mass volumes) by nullifying the corresponding meshes, so simulating the continuous removal of EL rock blocks and the retreat of the cliff slope (Fig. 6).

The outputs of the numerical modelling reveal that no failures occurred after the main fault dislodgement if an elasto-plastic behaviour is assumed, so demonstrating that the stress-release itself induced by tectonic activity is not sufficient to justify the lateral spreading observed (Fig. 2). On the contrary, such a process more likely evolved as a gravity-driven visco-plastic process, i.e. mainly controlled by the time-dependent rheology of the ductile EM below the stiff EL. The resulting displacement field reveals both vertical and horizontal displacements; the first one should be related to local sagging while the second ones justify the lateral involving the Siera de Aitana top slope. Cumulative strains within the EM in the horizontal direction (Fig. 7) create space of accommodation for the local sagging of EL blocks into the ductile EM where the vertical displacements mainly occur. Such a strain field is significantly controlled by the anticline-slope structure, since the displacement arrows have an opposite versus if considered from the hinge zone of the fold towards both the dip directions of the limb (Fig. 7).

The lateral spreading implies tensile stresses involving the EL slab as effect of the horizontal strains which are generated within the more ductile EM (Fig. 8a), so delimiting prismatic block which remain isolated by subvertical tension cracks evolving toward opened trenches. The resulting landform is a sequence of single rock blocks dislodged horizontally each other and separated by huge trenches where vertical sagging is locally arranged.

The initial failure of the stiff rock-cap results by the achievement of maximum strength along main joints (light blue indicator in Fig. 8b) which delimitate the rock-blocks of about 60–80 m in width (Fig. 8), i.e. fitting the field evidences collected at the Sierra de Aitana top ridge (Fig. 2a; see also Delgado et al., 2011). An antithetic joint set is generated respect to the grid interface which represents the main Sierra de Aitana fault, reproducing a conjugated fracturing associated with the

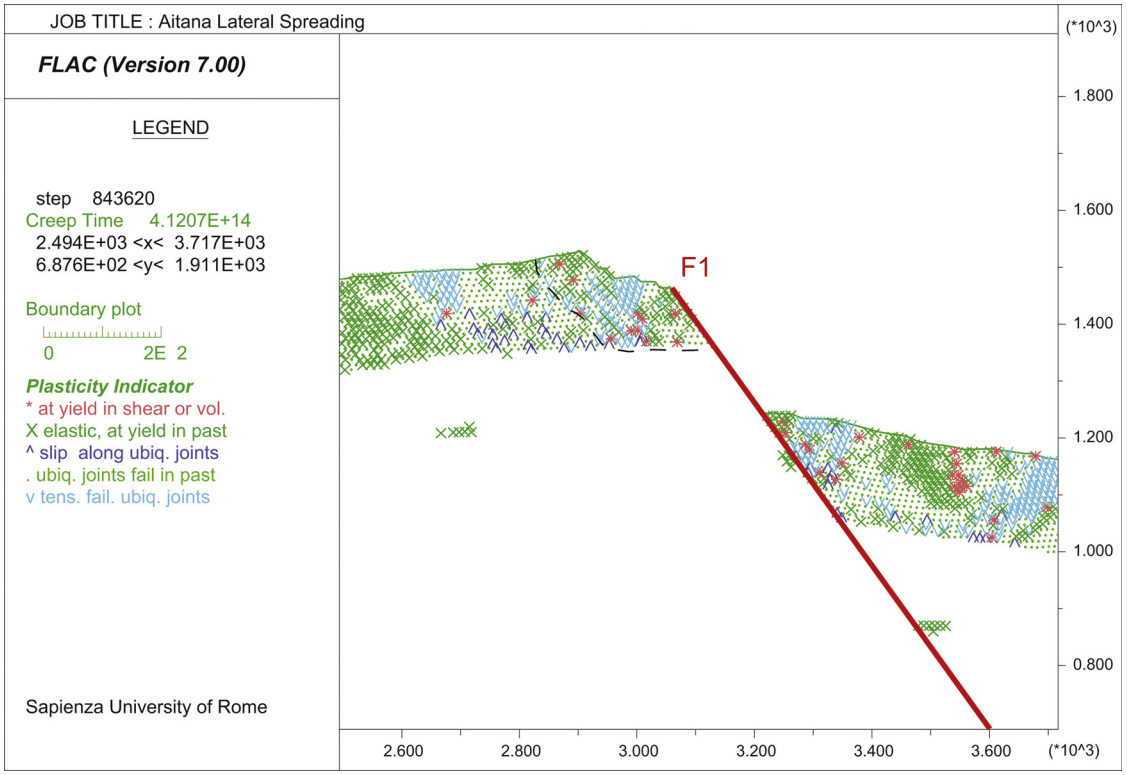

Fig. 6. Example of the adopted criterion for failed rock block removal. Plasticized volumes were removed where failed nodes envelope a portion kinematically free to move in lateral directions as results of fault displacement.

extensional displacements of the rock mass induced by the activity of the normal fault system (Fig. 8a).

The outputs of the parametric analysis performed by varying both the viscosity values of EM and the timing of activation of the secondary faults, highlighted a significant influence on: i) the trend of progressive deformation over time; ii) the resulting sequence of rock mass failures (coloured dots in Fig. 9); iii) number and distribution of the dislodged rock blocks.

The total cumulative deformations are directly related with the viscosity values assumptions (Fig. 9), resulting in a front retreat ranging between 50 and 450 m.

Under Hypothesis A and assuming a viscosity value of 10^{20} Pa·s (dark blue line in Fig. 9), an acceleration retreat rate was observed after the secondary faults activation. The front retreat appeared to be controlled by dislodgement of tectonic elements (F2-F3), which induce an increase in the relief energy and a sharp increase in strain rates. The

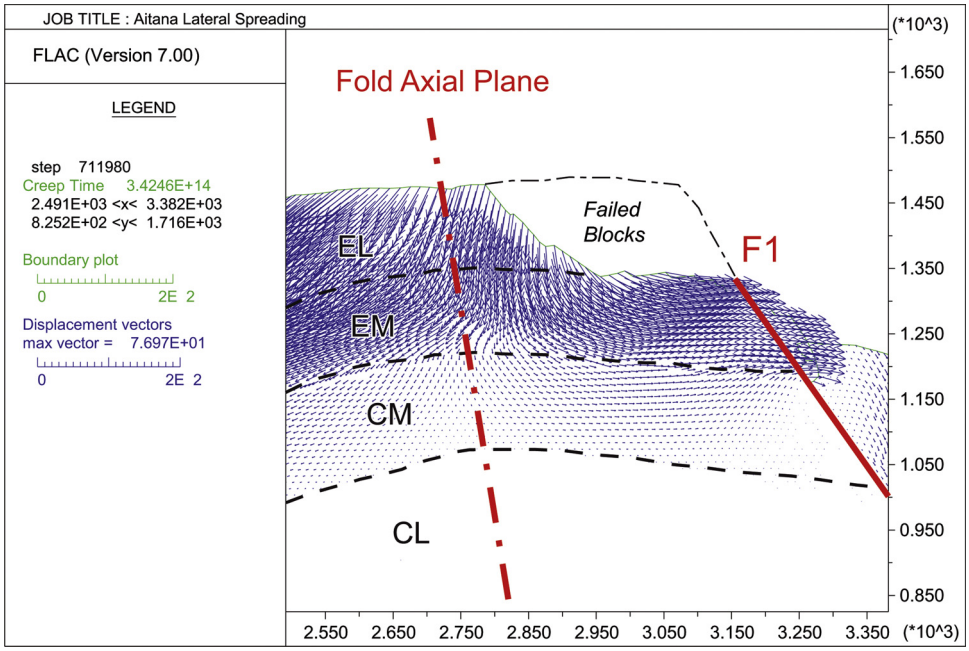

Fig. 7. Plot of displacement vectors (blue) resulting by lateral spreading process, which highlight the complex movement and the deformation pattern divergent from the anticline axial zone.

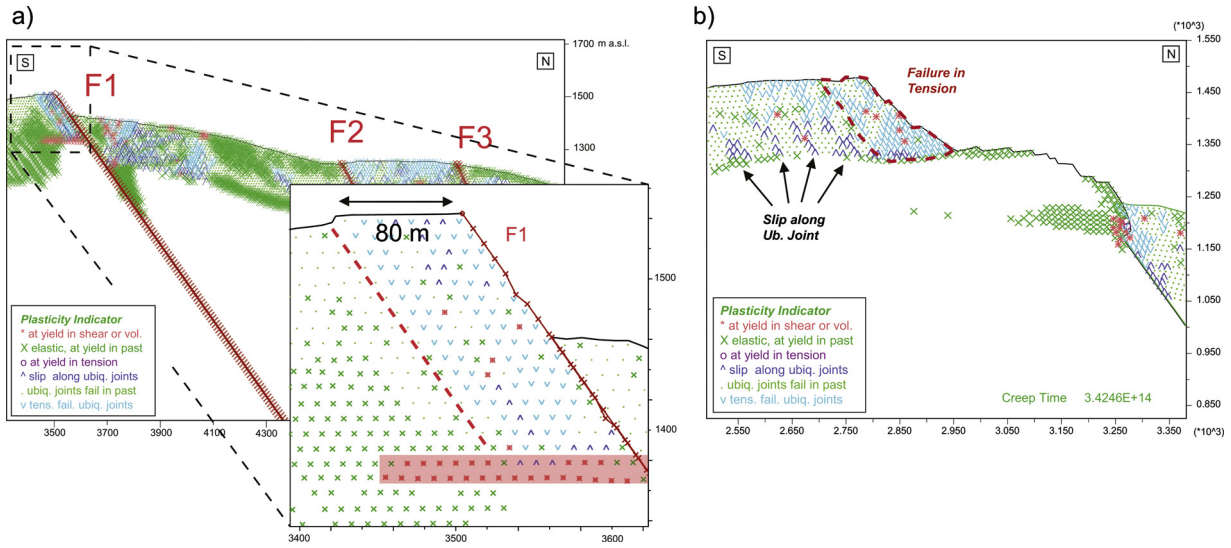

Fig. 8. a) First failure event occurred in the limestone slab (EL) as result of tensile stress induced by basal shearing within the more deformable EM (see inset plot). b) Example of induced plasticity plot in the last failure event. Maximum strength along ubiquitous joint (B) was reached isolating blocks under tensile failure of width of ~ 60–80 m.

activation of secondary faults induces an acceleration of the spreading process and subsequent failures, able to cause a total retreat of about 450 m (dark blue line in Fig. 9). Such an acceleration is evident only at the highest strain rates, where at least 4 rock failures occurred within hundreds of thousands of years (Fig. 9). In the following stages, the front retreat resulting by consecutive rock failure reduced its rate, cumulating failure over time with a rate consistent with ones observed before fault activation and under same viscosity values but different fault activation timing ("B" in Fig. 9).

If the highest viscosity values are assumed (10^{22} Pa·s), a minimum retreat of the Sierra de Aitana front equals to 50 m, results as a consequence of the lowest strain cumulated in EM (red line in Fig. 9). Similar results are obtained if intermediate viscosity values are attributed (i.e. ranging from 10^{21} Pa·s up to 5×10^{20} Pa·s). In this case, the resulting front retreat is about 175 m, as a consequence of failures of no more than two blocks (green and orange dots in Fig. 9), that does not justify the present cliff slope at the top of the Sierra de Aitana ridge.

Under the Hypothesis B and assuming a viscosity value of 10^{20} Pa·s (light blue line in Fig. 9), a similar acceleration retreat rate was observed after the secondary faults activation, postdating the ones obtained under Hypothesis A. The activation of secondary faults and the increased retreat rate cause a total retreat of about 350 m (light blue line in Fig. 9). In the following stages, in the last 1.5–2 Ma, the front retreat slows down after overtaking to the back-limb of the fold, with a rate consistent with ones observed under same viscosities solutions ("A" in Fig. 9). On the contrary, no relevant differences can be measured for higher viscosity values, where the cumulative horizontal displacements within the EM do not exceed few meters, inducing a stress state able to cause a limited front retreat with a rate not influenced at all by the activation of the Sierra de Aitana secondary faults.

The rheological best fit respect to the Sierra de Aitana lateral spreading resulted for a viscosity value of 10^{20} Pa·s, which justifies for both the Hypotheses A and B that the front retreat overtakes the fold axial plane, located about 250 m far from the Sierra de Aitana fault plane (see secondary y-axis on Fig. 9) as it results from the geological cross section of Fig. 3 and involving the back limb of the anticline fold. Such a rheological solution has a good fit with the long-term lateral spreading process, approaching the morphological target of the actual escarpment position under both the Hypotheses A and B of fault activation timing.

Nevertheless, only if the Hypothesis A is assumed, the total front retreat reached the total retreat target (Fig. 9), defined basing on a morphological criterion and fixed on the present shape of the cliff. Moreover, under this condition, after the last rock-block failure event, the modelling outputs evidences of incipient at yielding conditions for shearing along the joints (Fig. 8b). These results are in good agreement with the structural evidences of slipping along joints reported by Delgado et al. (2011); the related stress field is also coherent with the tension cracks which bound the fault escarpment in the EL formation all along the faulted Sierra de Aitana anticline (Delgado et al., 2011).

5. Discussion

The here obtained results highlight the relevant role of slope tectonics and inherited structural elements for regulating creep-driven rock mass slope deformations. Moreover, it is demonstrated a progressive evolution from a continuous-equivalent to a joint-driven rock mass mechanical behaviour, confirming how an initial pattern of joints and anisotropies leads to rock block dislodgment from a stable slope, allowing their progressive movement downhill (Fig. 8b).

In the Sierra de Aitana case study, the time-changing strain field is controlled by the structural setting of the local anticline, which diverges by the hinge zone following the symmetric limbs of the fold. The calibration of rock mass rheology was achieved by parametric approach back analysing the lateral spreading process by comparison with the expected mountain front retreat (Fig. 9).

The strain rates related to the lateral spreading process and induced by the progressive retreat of the ridge front as an effect of repeated block failures, are generally lower than 1–2 cm over thousands of years. Local acceleration of the retreat rates, exceeding 10 cm/kyr, only occurred if an equivalent rock mass viscosity of 10^{20} Pa·s is assumed as best-fit solution respect to the present target of ridge front retreat as well as to the morpho-structural observations reported in Delgado et al. (2011) and a fast retreat followed by the activation of secondary fault systems (F2-F3 of Figs. 4–9). No strain acceleration effects result from F2-F3 activation if different viscosity values are assumed.

In case of an early fault reactivation (Hypothesis A), time is enough for cumulating plastic deformation in EM formation inducing the EL rock-cap cracking under tensile stress which isolate huge prismatic blocks with a sizing comparable to the surveyed one (Fig. 2).

Basing on the obtained results, the back-analysis of the lateral spreading process was achieved only for a viscosity value of EM in the order of 10^{20} Pa·s. Such a value is in good agreement with previous studies (Esposito et al., 2007; Apuani et al., 2007; Bozzano et al., 2016;

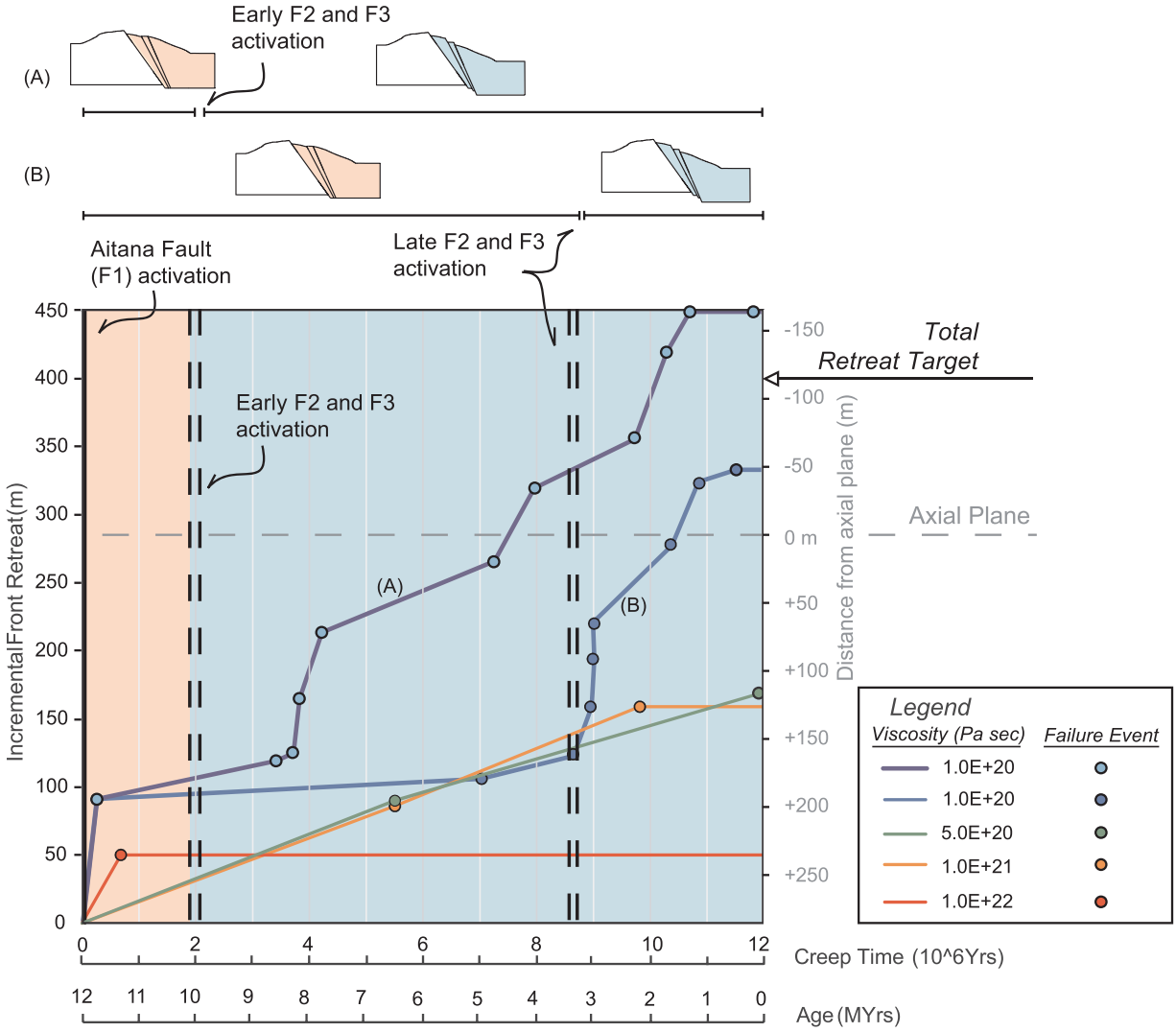

Fig. 9. Incremental front retreat vs. time under different viscosity assumptions resulting by the performed sensitivity analysis. Front retreat progress from the forelimb (positive values of secondary y-axis) towards the back limb by subsequent failure events (coloured dots). The results of timing of fault activation hypothesis (A, B) are reported for viscosity (η) $=10^{20}$ Pa·s. No relevant changes were derived at higher viscosity. (For interpretation of the references to colour in this figure, the reader is referred to the web version of this article.)

De Blasio and Martino, 2017; Della Seta et al., 2017). Since the irreversible strains, expressed by continuous creep-induced deformation, are strongly conditioned by the adopted time-dependent constitutive laws as well as by the values attributed to the rheological parameters which has been proved to be markedly time- and scale-dependent (Bretschneider et al., 2013), the rheological calibration of creep-driven processes can be mainly achieved by means of numerical modelling approaches.

The time-dependent modelling also allowed to evaluate the active and passive role of faults and folds in the time-evolution of large-scale lateral spreading, confirming the predisposing structural arrangement assessed by several authors in Apennines and Alps (Agliardi et al., 2001; Massironi et al., 2003; Jaboyedoff et al., 2011; Esposito et al., 2013).

It is worth noticing that the total amount of front retreat caused by subsequent failures does not consider effects due to weathering or erosion caused by periglacial process on the cap-rock during the whole modelled time interval. In addition, possible failures induced by transient input as seismic shaking were not considered in this study, even though several landslides were reported as triggered by historical earthquakes in the past (Delgado et al., 2006). For these reasons, basing on the cumulated total retreat with respect to the target, both the 10^{20} Pa·s solutions (Hypotheses A and B) are admissible solution to back-analyse the here considered process.

Possible role of dynamic actions, such as the ones that can be related to earthquakes experienced in past by the Sierra de Aitana region, was not considered in this study but cannot be excluded as probable perturbing external force. Such a kind of input can induce transient acceleration of the stationary creep, which could potentially evolve toward a tertiary stage corresponding to a generalised slope collapse, so anticipating the time-of-failure that should be expected due to the visco-plastic rheological behaviour. Ultimate scenarios of paroxysmal failure events occurred in past could have induced a continuous increase of the strain rate, causing a discontinuous increasing of cumulative deformations; nevertheless, this kind of scenarios in the study area is neither documented so far nor recorded by geological and geomorphological evidences.

6. Conclusions

Geological and structural setting as well as rheological features are proved to be the major predisposing factors in onset and evolution of slope-scale gravity induced processes, as testified by their deformational mechanisms, which prove the close relationship between a structural and geomorphological landscape evolution.

The here experienced multidisciplinary approach contributes to better understanding the structural control due to folds and faults on the ongoing lateral spreading process at Sierra de Aitana. Basing on the available knowledge about Neogene-Quaternary evolution of the External Zone of Betic Cordillera in Alicante region, a morpho-structural evolutionary model of the Sierra de Aitana faulted-anticline was constrained, reproducing by a sequential stress-strain numerical modelling the morpho-structural evolution of the slope which induced the observed lateral spreading.

The lateral spreading was back analysed: i) assuming as target the total front retreat comparable with the actual shape of the ridge; ii) considering a time-dependent creep process activated by the juxtaposition of EL over EM formation and iii) attributing a rock mass viscosity value in the order of 10^{20} Pa·s.

A last methodological result consisted in the numerical solution for simulating displacements along main fault planes by dislodging the numerical mesh through grid interfaces, which allowed to more realistically reproduce the morpho-structural evolution of slope-to-valley system, modelling through a multi-stage analysis their effect in timing major slope instabilities. This solution does not include the introduction of an artificial stress release as an effect of nullifying zones within the numerical domain. The here tested approached of disjointed domains of the numerical mesh revealed suitable for a detailed reproduction of fault activity in deforming slope system, opening new perspective for stress-strain analysis of past or ongoing slope instabilities evolving towards slope failure.

Author's contributions

PA, JD and FGT achieved the field survey and developed the morpho-evolutionary model. CE and GMM defined the engineering geological model. GMM and SM designed and perform the numerical modelling. GMM performed the laboratory experiments and analysed the numerical data. All authors contributed to discussions and interpretations of results.

Declaration of Competing Interest

None.

Acknowledgements

This research was funded in the frame of the project: "*Rock failures in cliff slopes: from back- to forward-analysis of processes through monitoring and multi-modelling approaches*" ("Sapienza" University of Rome, Italy-Year 2016, P.I. Prof. Salvatore Martino), "*Rock Mass Creeping, a multidisciplinary approach to characterize the long-term behaviour of faults and landslides*" ("Sapienza" University of Rome, Italy-Year 2017, P.I. Dott. Fabio Trippetta) and "*Evaluation of hazard associated to seismic-induced landslides*" (CGL2015-65602-R, MINECO-FEDER/EU, P.I. Prof. José Delgado). The authors wish to thank Francesca Pallone and Sara Dell'Unto for supporting data acquisition and laboratory investigations during their MD thesis. The authors also acknowledge, dr. Javier Martinez Martinez and Lucien Macone for their contributions in field sampling and laboratory testing.

References

Agliardi, F., Crosta, G., Zanchi, A., 2001. Structural constraints on deep-seated slope deformation kinematics. Eng. Geol. 59, 83–102. https://doi.org/10.1016/S0013-7952(00)00066-1.

Agliardi, F., Crosta, G.B., Zanchi, A., Ravazzi, C., 2009. Onset and timing of deep-seated gravitational slope deformations in the eastern Alps, Italy. Geomorphology 103, 113–129. https://doi.org/10.1016/j.geomorph.2007.09.015.

Ambrosi, C., Crosta, G.B., 2006. Large sackung along major tectonic features in the Central Italian Alps. Eng. Geol. 83, 183–200. https://doi.org/10.1016/j.enggeo.2005.06.031.

Apuani, T., Masetti, M., Rossi, M., 2007. Stress–strain–time numerical modelling of a deep-seated gravitational slope deformation: preliminary results. Quat. Int. 171, 80–89.

Ballantyne, C.K., 2002. Paraglacial geomorphology. Quat. Sci. Rev. 21, 1935–2017. https://doi.org/10.1016/S0277-3791(02)00005-7.

Barton, N., Choubey, V., 1977. The shear strength of rock joints in theory and practice. Rock Mech. 10 (1–2), 1–54.

Bianchi Fasani, G., Di Luzio, E., Esposito, C., Martino, S., Scarascia Mugnozza, G., 2011. Numerical modelling of Plio-Quaternary slope evolution based on geological constraints: a case study from the Caramanico Valley (Central Apennines, Italy). Geol. Soc. London Spec. Publ. 351, 201–214. https://doi.org/10.1144/SP351.11.

Bianchi Fasani, G., Di Luzio, E., Esposito, C., Evans, S.G., Scarascia Mugnozza, G., 2014. Quaternary, catastrophic rock avalanches in the Central Apennines (Italy): relationships with inherited tectonic features, gravity-driven deformations and the geodynamic frame. Geomorphology 211, 22–42.

Bois, T., Zerathe, S., Lebourg, T., Tric, E., 2015. Analysis of lateral rock spreading process initiation with a numerical modelling approach. Terra Nova 30, 369–379. https://doi.org/10.1111/ter.12352.

Borgatti, L., Guerra, C., Nesci, O., Romeo, R.W., Veneri, F., Landuzzi, A., Benedetti, G., Marchi, G., Lucente, C.C., 2015. The 27 February 2014 San Leo landslide (northern Italy). Landslides 12, 387–394. https://doi.org/10.1007/s10346-015-0559-4.

Bozzano, F., Bretschneider, A., Martino, S., 2008. Stress-strain history from the geological evolution of the Orvieto and Radicofani cliff slopes (Italy). Landslides 5, 351–366. https://doi.org/10.1007/s10346-008-0127-2.

Bozzano, F., Martino, S., Prestininzi, A., 2010. Ruolo dell'assetto geologico sulle condizioni di stabilità della collina di Gerace (Reggio Calabria, Italia). Ital. J. Geosci. 129, 280–296. https://doi.org/10.3301/IJG.2010.10.

Bozzano, F., Martino, S., Montagna, A., Prestininzi, A., 2012. Back analysis of a rock landslide to infer rheological parameters. Eng. Geol. 131–132, 45–56. https://doi.org/10.1016/j.enggeo.2012.02.003.

Bozzano, F., Bretschneider, A., Esposito, C., Martino, S., Prestininzi, A., Scarascia Mugnozza, G., 2013. Lateral spreading processes in mountain ranges: insights from an analogue modelling experiment. Tectonophysics 605, 88–95.

Bozzano, F., Della Seta, M., Martino, S., 2016. Time-dependent evolution of rock slopes by a multi-modelling approach. Geomorphology 263, 113–131. https://doi.org/10.1016/j.geomorph.2016.03.031.

Bretschneider, A., Genevois, R.A., Martino, S., Prestininzi, A., Verbena, G.S., 2013. A physically-based scale approach to the analysis of the creep process involving Mt. Granieri (Southern Italy). Ital. J. Eng. Geol. Environ. 2013, 123–131. https://doi.org/10.4408/IJEGE.2013-06.B-09.

Canuti, P., Casagli, N., Garzonio, C.A., Vannocci, P., 1990. Lateral spreads and landslide hazards in the Northern Apennine: the example of the Mt. Fumaiolo (Emilia-Romagna) and Chiusi della Verna (Tuscany). Proceedings 6th Congr. IAEG, Amsterdam 1525–1533 3.

De Blasio, F.V., Martino, S., 2017. The Acheron Dorsum on Mars: a novel interpretation of its linear depressions and a model for its evolution. Earth Planet. Sci. Lett. 465, 92–102. https://doi.org/10.1016/j.epsl.2017.02.019.

Delgado, J., Peláez, J.A., Tomás, R., Estévez, A., López Casado, C., Doménech, C., Cuenca, A., 2006. Evaluación de la susceptibilidad de las laderas a sufrir inestabilidades inducidas por terremotos: Aplicación a la cuenca de drenaje del río Serpis (provincia de Alicante). Rev. Soc. Geol. Esp. 19, 197–218.

Delgado, J., Vicente, F., García-Tortosa, F., Alfaro, P., Estévez, A., Lopez-Sanchez, J.M., Tomás, R., Mallorquí, J.J., 2011. A deep seated compound rotational rock slide and rock spread in SE Spain: structural control and DInSAR monitoring. Geomorphology 129, 252–262. https://doi.org/10.1016/j.geomorph.2011.02.019.

De Ruig, M.J., 1992. Tectono-sedimentary Evolution of the Prebetic Fold Belt of Alicante (SE Spain). A Study of Stress Fluctuations and Foreland Basin Deformation. PhD Thesis. Amsterdam University.

Della Seta, M., Esposito, C., Marmoni, G.M., Martino, S., Scarascia Mugnozza, G., Troiani, F., 2017. Morpho-structural evolution of the valley-slope systems and related implications on slope-scale gravitational processes: new results from the Mt. Genzana case history (Central Apennines, Italy). Geomorphology 289, 60–77. https://doi.org/10.1016/j.geomorph.2016.07.003.

Di Luzio, E., Bianchi Fasani, G., Saroli, M., Esposito, C., Cavinato, G.P., Scarascia Mugnozza, G., 2004a. Massive rock slope failure in the central Apennines (Italy): the case of the Campo di Giove rock avalanche. Bull. Eng. Geol. Environ. 63, 1–12. https://doi.org/10.1007/s10064-003-0212-7.

Di Luzio, E., Saroli, M., Esposito, C., Bianchi Fasani, G., Cavinato, G.P., Scarascia Mugnozza, G., 2004b. Influence of structural framework on mountain slope deformation in the Maiella anticline (Central Apennines, Italy). Geomorphology 60, 417–432. https://doi.org/10.1016/j.geomorph.2003.10.004.

Discenza, M.E., Esposito, C., Martino, S., Petitta, M., Prestininzi, A., Scarascia Mugnozza, G., 2011. The gravitational slope deformation of Mt. Rocchetta ridge (central Apennines, Italy): geological-evolutionary model and numerical analysis. Bull. Eng. Geol. Environ. 70, 559–575. https://doi.org/10.1007/s10064-010-0342-7.

Esposito, C., Martino, S., Scarascia Mugnozza, G., 2007. Mountain slope deformations along thrust fronts in jointed limestone: an equivalent continuum modelling approach. Geomorphology 90, 55–72. https://doi.org/10.1016/j.geomorph.2007.01.017.

Esposito, C., Bianchi Fasani, G., Martino, S., Scarascia Mugnozza, G., 2013. Quaternary gravitational morpho-genesis of Central Apennines (Italy): insights from the Mt. Genzana case history. Tectonophysics 605, 96–103. https://doi.org/10.1016/j.tecto.2013.06.023.

Esposito, C., Di Luzio, E., Scarascia Mugnozza, G., Bianchi Fasani, G., 2014. Mutual interactions between slope-scale gravitational processes and morpho-structural evolution of central Apennines (Italy): review of some selected case histories. Rend. Fis. Acc. Lincei 25 (Suppl 2), 151. https://doi.org/10.1007/s12210-014-0348-3.

Hoek, E., Carranza-Torres, C.T., Corkum, B., 2002. Hoek-Brown failure criterion-2002 edition (PDF). Proceedings of the Fifth North American Rock Mechanics Symposium 267–273 1.

Hungr, O., Leroueil, S., Picarelli, L., 2014. The Varnes classification of landslide types, an update. Landslides 11, 167–194. https://doi.org/10.1007/s10346-013-0436-y.

Hutchinson, J.N., 1988. General report: morphological and geotechnical parameters of landslides in relation to geology and hydrogeology. In: Ch, Bonnard (Ed.), Landslides. Proc 5th Int Symp on Landslides. AA Balkema, Rotterdam. pp. 3–35.

I.S.R.M, 1978. Suggested methods for the quantitative description of discontinuities in rock masses. Int. J. Rock Mech. Min. Sci. Geomech. Abstracts 15, 319–368.

Jaboyedoff, M., Oppikofer, T., Derron, M.H., Blikra, L.H., Böhme, M., Saintot, A., 2011. Complex landslide behaviour and structural control: a three-dimensional conceptual model of Åknes rockslide, Norway. Geol. Soc. London Spec. Publ. 351, 147–161. https://doi.org/10.1144/SP351.8. 30 March 2011.

Kellogg, K.S., 2001. Tectonic controls on large landslide complex: Williams Fork Mountains near Dillon, Colorado. Geomorphology 41, 355–368. https://doi.org/10.1016/S0169-555X(01)00067-8.

Marco Molina, J.A., 1990. Aitana, análisis morfoestructural. Instituto Universitario de Geografía-Universidad de Alicante e Instituto de Cultura "Juan Gil-Albert"-Diputación Provincial de Alicante.

Marmoni, G.M., 2011. Laboratory and Field Geomechanical Characterization of Eocene Limestone of the Sierra De Aitana, Alicante (Spain). Master Thesis.

Marmoni, G.M., Martino, S., Heap, M.J., Reuschlé, T., 2017. Gravitational slope-deformation of a resurgent caldera: new insights from the mechanical behaviour of Mt. Nuovo tuffs (Ischia Island, Italy). J. Volcanol. Geotherm. Res. 345, 1–20. https://doi.org/10.1016/j.jvolgeores.2017.07.019.

Martino, S., Della Seta, M., Esposito, C., 2017. Back-analysis of rock landslides to infer rheological parameters. Xia-Ting Feng. Rock Mechanics and Engineering. Volume 3: Analysis, Modeling & Design. Taylor & Francis, London (UK), pp. 237–267 ISBN: 978-1-138-02761-9.

Massironi, M., Bistacchi, A., Dal Piaz, G.V., Monopoli, B., Schiavo, A., 2003. Structural control on mass-movement evolution: a case study from the Vizze Valley, Italian Eastern Alps. Eclogae Geol. Helv. 96, 85–98.

Pasuto, A., Soldati, M., 1996. Rock spreading. In: Dikau, R., Brunsden, D., Schrott, L., Ibsen, M.-L. (Eds.), Landslide Recognition: Identification, Movement and Causes. Wiley, Chichester, pp. 122–136.

Ramamurthy, T., 1994. Strength and modulus responses of anisotropic rocks. In: In: Hudson, J.A. (Ed.), Comprehensive Rock Engineering, vol. 1. Pergamon Press, Oxford, pp. 313–329.

Rey, J., Fumanal, M.P., 1996. Cuaternario submarino frente a la Serra Gelada (Alicante) y sus implicaciones eustático-paleogeográficas. Cuad. Geogr. Univ. Valencia 60, 243–258.

Rohn, J., Resch, M., Schneider, H., Fernandez-Steeger, T.M., Czurda, K., 2004. Large-scale lateral spreading and related mass movements in the Northern Calcareous Alps. Bull. Eng. Geol. Environ. 63, 71–75. https://doi.org/10.1007/s10064-003-0201-x.

Roselló, V.M., Fumanal, M.P., 1999. Climbing dunes and interbedded rubble fans. Quaaternary patterns of Serra Gelada (spanish Mediterranean littoral). Z. Geomorphol. N.F. 43, 235–254.

Sanz de Galdeano, C., Alfaro, P., 2004. Tectonic significance of the present relief of the Betic Cordillera. Geomorphology 63, 175–190.

Scarascia Mugnozza, G., Bianchi Fasani, G., Esposito, C., Saroli, M., Di Luzio, E., Evans, S.G., et al., 2006. Rock avalanche and Mountain slope deformation. In: Evans, S.G. (Ed.), Landslides from Massive Rock Slope Fail. Landslides, pp. 357–376.

Sitharam, T.G., Sridevi, J., Shimizu, N., 2001. Practical equivalent continuum characterization of jointed rock masses. Int. J. Rock Mech. Min. Sci. 38, 437–448. https://doi.org/10.1016/S1365-1609(01)00010-7.

Spreafico, M.C., Cervi, F., Francioni, M., Stead, D., Borgatti, L., 2017. An investigation into the development of toppling at the edge of fractured rock plateaux using a numerical modelling approach. Geomorphology 288, 83–98. https://doi.org/10.1016/j.geomorph.2017.03.023.

Sridevi, J., Sitharam, T.G., 2000. Analysis of strength and moduli of jointed rocks. Geotech. Geol. Eng. 18, 3–21. https://doi.org/10.1023/A:1008992621515.

Varnes, D.J., 1978. Slope movement types and processes. Special Report 176, 11–33.

Yébenes, A., Alfaro, P., Delgado, J., Estévez, A., Soria, J.M., 2002. Sea cliffs resulting from late Miocene extensional tectonics: the Serra Gelada case study (Betic Cordillera, Spain). Geomorphology 42, 197–211.